

Geophysical Research Letters*



RESEARCH LETTER

10.1029/2025GL116311

Key Points:

- A new atomic hydrogen data set based on SCIAMACHY OH airglow measurements in the mesopause region is presented
- The retrieval involves minimal kinetic and spectroscopic parameters, reducing uncertainty in the derived atomic hydrogen number density
- The new data set differs by over 30% from previous H data sets, but shows better agreement with in situ measurements

Correspondence to:

Y. Zhu, y.zhu@swl.ac.cn

Citation

Wu, X., Zhu, Y., Smith, A. K., Kaufmann, M., & Xu, J. (2025). Nighttime atomic hydrogen abundance retrieved from SCIAMACHY hydroxyl airglow measurements in the mesopause region. *Geophysical Research Letters*, 52, e2025GL116311. https://doi.org/10.1029/2025GL116311

Received 4 APR 2025 Accepted 25 JUL 2025

Author Contributions:

Conceptualization: Xiaolin Wu,

Yajun Zhu
Data curation: Xiaolin Wu, Yajun Zhu
Formal analysis: Xiaolin Wu
Funding acquisition: Yajun Zhu
Investigation: Xiaolin Wu, Yajun Zhu
Methodology: Xiaolin Wu, Yajun Zhu
Resources: Yajun Zhu
Software: Xiaolin Wu, Yajun Zhu
Supervision: Yajun Zhu
Validation: Xiaolin Wu
Visualization: Xiaolin Wu

Writing - original draft: Xiaolin Wu

Yajun Zhu, Anne K. Smith,

Martin Kaufmann, Jiyao Xu

Writing - review & editing: Xiaolin Wu,

© 2025 The Author(s).

This is an open access article under the terms of the Creative Commons

Attribution-NonCommercial License, which permits use, distribution and reproduction in any medium, provided the original work is properly cited and is not used for commercial purposes.

Nighttime Atomic Hydrogen Abundance Retrieved From SCIAMACHY Hydroxyl Airglow Measurements in the Mesopause Region

Xiaolin Wu^{1,2}, Yajun Zhu^{1,3}, Anne K. Smith⁴, Martin Kaufmann⁵, and Jiyao Xu^{1,3}

¹State Key Laboratory of Solar Activity and Space Weather, National Space Science Center, Chinese Academy of Sciences, Beijing, China, ²College of Earth and Planetary Sciences, University of Chinese Academy of Sciences, Beijing, China, ³Hainan National Field Science Observation and Research Observatory for Space Weather, Hainan, China, ⁴NSF National Center for Atmospheric Research, Boulder, CO, USA, ⁵Institute of Climate and Energy Systems - Stratosphere (ICE-4), Forschungszentrum Jülich, Jülich, Germany

Abstract Atomic hydrogen (H) is crucial for understanding photochemistry and the energy budget in the mesopause region. However, there is still no consensus on the H abundance in this region. This study presents a new hydrogen data set derived from Scanning Imaging Absorption Spectrometer for Atmospheric Chartography (SCIAMACHY) OH(9–6) band spectra, collocated with temperature and ozone profiles from other remote sensing instruments. H number densities peak at 82–87 km and range from 1.5 × 10⁸ to 4 × 10⁸ cm⁻³, depending on season and latitude. Two other H data sets obtained from the Sounding of the Atmosphere using Broadband Emission Radiometry (SABER) are presented for comparison: those from Mlynczak et al. (2018, https://doi.org/10.1029/2018GL077377) and Panka et al. (2021, https://doi.org/10.1029/2020GL091053) are approximately 30% lower and 50% higher than the SCIAMACHY data at peak altitudes, respectively. Additionally, the H number density retrieved in this study partly shows better agreement with the only direct rocket in situ measurements than those from SABER.

Plain Language Summary Atomic hydrogen (H) plays a crucial role in photochemistry and energy balance in the mesopause region. However, the exact number density of atomic hydrogen ([H]) remains uncertain. With the development of the relaxation mechanism of vibrationally excited OH and a broad set of satellite data, we present a new atomic hydrogen data set derived from Scanning Imaging Absorption Spectrometer for Atmospheric Chartography (SCIAMACHY) OH(9–6) band spectra, collocated with temperature and ozone profiles from other remote sensing instruments. Our results show that atomic hydrogen peaks at altitudes of 82–87 km, with number densities ranging from 1.5×10^8 to 4×10^8 cm⁻³, varying with season and latitude. The [H] retrieved in this study lies between the values derived from Mlynczak et al. (2018, https://doi.org/10.1029/2018GL077377) and Panka et al. (2021, https://doi.org/10.1029/2020GL091053) at peak altitudes, with biases of 30% and 50%, respectively. Furthermore, our retrieved [H] is partly consistent with the only direct rocket in situ observation.

1. Introduction

Atomic hydrogen (H) plays an important role in photochemistry and energy balance in the upper mesosphere and lower thermosphere (UMLT) region (Mlynczak & Solomon, 1991, 1993), which spans altitudes of approximately 80–120 km. This trace gas is primarily produced by the photolysis of water vapor and undergoes a highly exothermic reaction with ozone (O_3), directly producing vibrationally excited hydroxyl at v = 5–9 states, and serving as one of the largest sources of heat in the mesopause region (Mlynczak & Solomon, 1991; Mlynczak et al., 2014). Therefore, quantifying atomic hydrogen density is crucial for clarifying the role of H-related chemical reactions in the energy budget. Moreover, H is involved in numerous chemical reactions, therefore accurate atomic hydrogen abundance is indispensable for the retrieval of several constituents, such as HO_2 and OH (Kulikov et al., 2022).

Detecting H at the mesopause region is very difficult. Due to its low density, it is challenging for in situ measurements to capture hydrogen in this region. The only direct in situ measurements were carried out by Sharp and Kita (1987) using the resonance lamp technique on board a rocket. Remote sensing techniques are also difficult to apply because hydrogen lacks a permanent dipole moment, and many transitions are forbidden by quantum

WU ET AL.

mechanical selection rules. Therefore hydroxyl emissions from the reaction between atomic hydrogen and ozone are commonly used as a proxy for atomic hydrogen abundance. Kaufmann et al. (2013) used the data from the OH (9–6) vibrational band, measured by the Scanning Imaging Absorption Spectrometer for Atmospheric Chartography (SCIAMACHY), alongside ozone limb measurements from the Global Ozone Monitoring by Occultation of Stars (GOMOS) instrument, to derive atomic hydrogen abundance. Since then, significant updates to the OH non-LTE model have improved our understanding, thereby reducing uncertainties related to the model coefficients. Additionally, total atmospheric number density was previously taken from the MSISE-00 model instead of measurements, which introduced further uncertainties. Given these advancements, it appears worthwhile to revisit and update this data set to enhance its accuracy and reliability.

Two other atomic hydrogen data sets published in recent years are based on measurements of the OH volume emission rates at 2.0 µm from the Sounding of the Atmosphere using Broadband Emission Radiometry (SABER) instrument. These data sets were used to derive hydrogen abundance based on different OH emission mechanisms (Kulikov et al., 2024; Mlynczak et al., 2014, 2018). Although various atomic hydrogen data sets agree on the overall profile shape, discrepancies remain, particularly regarding the abundance at the peak.

To contribute to ongoing discussions, we present a new hydrogen data set based on SCIAMACHY OH measurements. Moreover, this work focuses on comparing the different hydrogen data sets and analyzing their differences.

2. Data

SCIAMACHY was a multi-channel grating spectrometer onboard Envisat (Bovensmann et al., 1999) that operated from 2002 to 2012. It included eight spectral channels covering the spectral range from 220 to 2,400 nm, with a channel-dependent spectral resolution ranging from 0.2 to 1.5 nm (Gottwald et al., 2006). Envisat operated in a sun-synchronous orbit, crossing the equator at local solar times of 10:00 a.m. and 10:00 p.m. In nighttime limb-viewing mode, the tangent altitudes of the line of sight for SCIAMACHY ranged between approximately 73 and 148 km, with altitude steps of 3.3 km. Mesospheric limb observations spanned latitudes from 30°S to 50°N and from 0° to 80°N during the night side (Kaufmann et al., 2008). In this work, we focus on the OH(9–6) near-infrared spectra, with wavelengths between 1,377 and 1,400 nm at a resolution of 1.5 nm from channel 6, at a local solar time of 10:00 p.m.

Because the SCIAMACHY instrument was unable to simultaneously measure ozone, temperature, and total density in the UMLT during nighttime, we rely on SABER (V2.0) measurements for these data. The ozone data from GOMOS is also used for comparison. To enhance the signal-to-noise ratio, monthly zonal median data in 5° latitude bins were used before retrieval. Although averaging measurements prior to inversion may introduce additional errors due to the nonlinear dependence of the expression for H on input data, our assessment shows that the resulting bias is relatively small (5%–10%) and will be taken into account in the total uncertainty analysis. The coincidence criteria were $\pm 2.5^{\circ}$ in latitude and 1 hr in local time. The N_2 and O_2 mixing ratio was determined from the MSIS 2.0 (Emmert et al., 2021).

3. Retrieval of Nighttime Atomic Hydrogen

The volume emission rate (VER) of OH(9–6) ro-vibrational lines measured by SCIAMACHY comes directly from the reaction of H + O₃. Assuming the hydroxyl state OH(ν = 9) is in chemical equilibrium (Xu et al., 2012), the number density of hydrogen ([H]) can be expressed as:

[H] =
$$\frac{VER \cdot (A_9 + k_{O,9} \cdot [O] + k_{O_2,9} \cdot [O_2] + k_{N_2,9} \cdot [N_2])}{f_9 \cdot k_1 [O_3] \cdot A_{96}}$$
(1)

where k_1 represents the rate constant for the reaction H + O₃, f_9 is the branching ratio of OH($\nu=9$) for H + O₃, taken as 0.47 (Adler-Golden, 1997). A_9 represents the total spontaneous emission rate for OH($\nu=9$) and A_{96} is the sum of the Einstein coefficient of the ro-vibrational lines within the 9–6 band considered. They are both taken from the HITRAN-2012 database (Rothman et al., 2013). Additionally, differences compared to HITRAN-2020 (Gordon et al., 2022), are discussed below in terms of their impact on our retrieval. The terms $k_{O_2,9}$ and $k_{N_2,9}$ denote the total quenching rates of OH($\nu=9$) with O₂ and N₂, respectively. $k_{O,9}$ is the sum of chemical and

WU ET AL. 2 of 9

Parameter	Value	Reference
k_1	$1.4 \times 10^{-10} \exp(-470/T) \mathrm{cm}^3/\mathrm{s}$	Burkholder et al. (2020)
k_2	$6.1 \times 10^{-34} (298/T)^{2.4} \mathrm{cm}^6/\mathrm{s}$	Burkholder et al. (2020)
k_3	$8 \times 10^{-12} \exp(-2060/T) \mathrm{cm}^3/\mathrm{s}$	Burkholder et al. (2020)
f_9	0.47	Adler-Golden (1997)
$k_{\mathrm{O}_2,9}$	$1.18 \times 2.2 \times 10^{-11} \mathrm{cm}^3/\mathrm{s}$	Kalogerakis et al. (2011) and Panka et al. (2017)
$k_{N_2,9}$	$1.4 \times 7 \times 10^{-13} \mathrm{cm}^3/\mathrm{s}$	Kalogerakis et al. (2011) and Lacoursière et al. (2003)
k_{O}	$2.3 \times 10^{-10} \mathrm{cm}^3/\mathrm{s}$	Sharma et al. (2015)

collisional quenching rates of OH(v = 9) with O. The removal rate constants, shown in Table 1, are identical to those used by Zhu and Kaufmann (2018). The square brackets indicate the number density of the corresponding chemical species. The number density of atomic oxygen ([O]) can be expressed as a function related to [H] through the ozone balance equation:

$$[O] = \frac{k_1 \cdot [H] \cdot [O_3]}{k_2 \cdot [O_2] \cdot [M] - k_3 \cdot [O_3]}$$
 (2)

In Equation 2, k_1 and k_3 are the rate constants for the reactions of O_3 with H and O, respectively. k_2 represents the rate constant for recombination reaction $O + O_2 + M$. M represents the background atmosphere. The values of these rate constants are taken from Burkholder et al. (2020).

By combining Equations 1 and 2, we derived the distribution of [H] based on SCIAMACHY OH(9-6) band emission measurements.

4. Results and Discussions

A systematic error analysis was performed on the retrieved [H]. The main sources of uncertainty are the background atmospheric parameters, mainly temperature and O_3 , and the collisional parameters $k_{O,9}$, $k_{O,9}$, and $k_{N,9}$. SABER temperature uncertainties are around 2 K at 80 km and 7.5 K at 96 km, which is the primary uncertainty factor in the retrieval of O at its peak altitude (Zhu & Kaufmann, 2018). However, it has only a minor effect on the inversion of [H], approximately 5%, because the temperature-induced variations in k_1 , k_2 , and k_3 effectively cancel each other out through a complex equation involving [H] (as governed by Equations 1 and 2). The differences between the SABER and GOMOS ozone data sets are used to estimate the ozone uncertainty. Since the SABER O₃ data are 15%-25% higher than the GOMOS data, a 20% ozone uncertainty is applied, which affects the derived [H] by approximately 20%. The uncertainties of collisional rates for OH(v = 9) in collision with O, O_2 , N_2 are taken as $(2.3 \pm 1) \times 10^{-10}$ cm³/s, $(2.2 \pm 0.6) \times 10^{-11}$ cm³/s, $(7 \pm 2) \times 10^{-13}$ cm³/s (Kalogerakis et al., 2011; Zhu & Kaufmann, 2018). The change in $k_{0.9}$ has almost no effect on [H] at 80–83 km but causes about a 15% effect at 96 km. The influence of $k_{0.9}$ decreases with increasing altitude, from about 20% at 80 km to 10% at 80 km to 10% at 80 km. at 96 km. The influence of N2 is minimal (no more than 3%). In addition, applying monthly zonal median averaging to spectra data prior to retrieval introduces an additional uncertainty of approximately 5% above 85 km and 10% at 80-83 km. Assuming the parameters are independent, we calculate the total uncertainty by taking the root-sum-square (RSS) of each individual variation. The total uncertainty is approximately 25%-32% at 80-96 km, primarily driven by the uncertainties in O_3 and k_{O_3} . Finally, we evaluate the impact of the $O + O_3$ reaction on the retrieval of [H]. We find that neglecting this reaction leads to a decrease in [H] of no more than 5% at 80-96 km, which is minimal.

The Einstein coefficients from HITRAN-2020 are about 17% lower than those from HITRAN-2012 at OH(9–6) emission band. By comparing the [H] derived from these two HITRAN data sets, we find that the [H] data set retrieved from HITRAN-2020 is about 17% larger than that from HITRAN-2012. Further studies on the HITRAN hydroxyl Einstein coefficients are needed, but it is beyond the focus of this work. In the following analysis,

WU ET AL. 3 of 9

19448007, 2025, 15, Downloa

ded from https://agupubs.onlinelibrary.wiley.com/doi/10.1029/2025GL116311 by Forschungszentrum Jülich GmbH Research Center, Wiley Online Library on

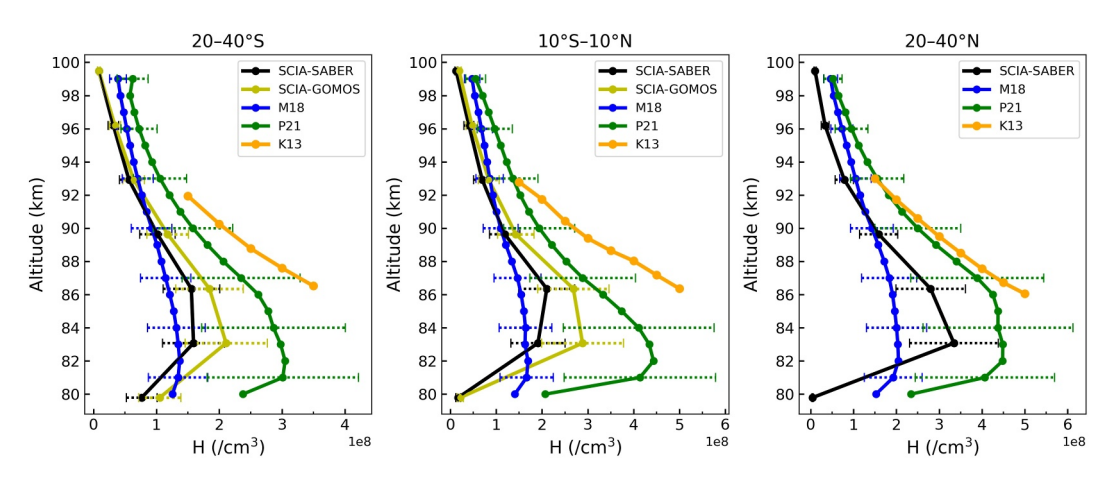


Figure 1. The zonal mean atomic hydrogen abundance for June, July, and August 2008 for 20° – 40° S (left), 10° S– 10° N (middle), and 20– 40° N (right). SCIA-SABER and SCIA-GOMOS indicate the [H] derived from SCIAMACHY OH(9–6) band emission in this work, using O_3 data from SABER and GOMOS, respectively. At 20° – 40° N (right), there are no GOMOS O_3 data. M18 is the [H] derived from the SABER 2 μ m OH channel following Mlynczak et al. (2018), while P21 is the [H] derived from Panka et al. (2021). K13 is the [H] derived from Kaufmann et al. (2013). The horizontal dotted lines represent uncertainty estimates. For SCIA-SABER and SCIA-GOMOS, the uncertainties are calculated as described in the uncertainty analysis section. For M18 and P21, the uncertainties are obtained from Mlynczak et al. (2014) and Panka et al. (2021), respectively.

HITRAN-2012 is used to retrieve [H], ensuring comparability with previous [H] data sets under relatively consistent conditions.

Panka et al. (2021) obtained nighttime [O] and densities of different OH vibrational levels from two OH emission channels at 2 μ m and 1.6 μ m measured by SABER, all of which are available on the SABER website. We use the photochemistry equilibrium of OH($\nu = 9$) and its number density to determine the [H] for comparison, which is referred to as P21 in this work, with atmospheric input parameters and rate constants consistent with those of Panka et al. (2021).

Figure 1 shows our retrieved atomic hydrogen abundance across different latitude bands for June, July, and August 2008, with the other hydrogen data sets included for comparison. SCIA-SABER and SCIA-GOMOS represent the [H] data sets obtained from SCIAMACHY OH(9-6) emission with O₃ data from SABER and GOMOS, respectively. M18 indicates the [H] data set derived from SABER OH channel at 2 µm (Mlynczak et al., 2018), while P21 represents the [H] data derived from Panka et al. (2021). K13 represents the [H] data obtained from Kaufmann et al. (2013). At 20°-40°S and 10°S-10°N, SCIA-SABER and SCIA-GOMOS differ by about 15% above 90 km and 20%-30% below 90 km because GOMOS O₃ data is 15%-30% lower than SABER O₃ data. At the peak altitude of 82–87 km, M18 is about 15%–40% lower than SCIA-SABER. Above 90 km and at 80-82 km, M18 show higher abundance compared to the [H] derived from SCIAMACHY. Nevertheless, the two data sets are consistent within their respective uncertainties over 82-96 km. Note that the ozone chemical equilibrium boundary is about 82–83 km at low latitudes (Kulikov et al., 2023), which may be a source of error in our calculations and those of M18 below about 82 km. The P21 data set is significantly higher than both SCIA-SABER and M18 across the entire altitude profile. Compared to SCIA-SABER, P21 is 50%-100% higher at 82-87 km, except at 20-40°N, where it is 35% higher at 83 km. However, SCIA-GOMOS agrees with P21 between 83 and 96 km when considering the uncertainty of P21. Furthermore, applying the Einstein coefficients from HITRAN-2020 would increase SCIA-GOMOS values by about 17%, making it closer to P21. The [H] from Kaufmann et al. (2013) is much larger than the other data sets. At 90 km, it is approximately 90% larger than SCIA-GOMOS, as shown in Figure 1. Based on calculations, the systematic discrepancy between the K13 and SCIA-GOMOS data sets at 90 km from 2003 to 2008 is around 60%.

The spatial distribution of atomic hydrogen number density derived from SCIAMACHY OH(9–6) emission and SABER O_3 for 2005 is presented in Figure 2. The peak altitude is between 82 and 87 km, with number densities ranging from 1.5×10^8 to 4×10^8 cm⁻³, varying with latitude and season. The annual mean atomic hydrogen number density in the equatorial region is about 2×10^8 cm⁻³, peaking around 83 km.

WU ET AL. 4 of 9

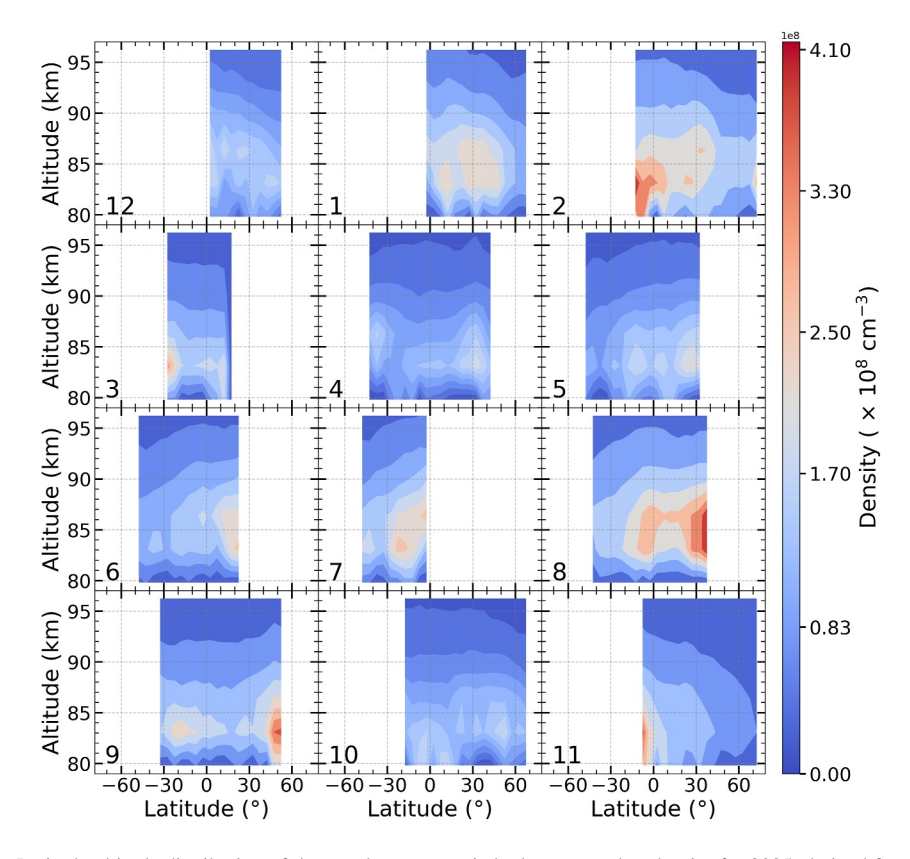


Figure 2. Latitude-altitude distribution of the zonal mean atomic hydrogen number density for 2005, derived from SCIAMACHY OH(9–6) data and SABER ozone data. The numbers represent the month of the year.

The differences between SCIA-SABER and M18 by latitude and month are shown in Figure 3 (top). Between 82 and 90 km, M18 is 30% lower than SCIA-SABER on average. However, above 90 km, M18 is 10%–50% higher than the SCIA-SABER data. This difference increases with increasing altitude. Below 82 km, where the ozone chemical balance does not hold, M18 values are sometimes more than 50% higher than SCIA-SABER. In contrast, the [H] derived from Panka et al. (2021) are generally higher than SCIA-SABER at almost all altitudes (Figure 3, bottom). Between 83 and 90 km, they are approximately 50% higher on average. Above 90 km, the relative difference exceeds 50% and increases with altitude, reaching up to 100% at 96 km.

The results above show significant discrepancies between the different [H] data sets. It is essential to explore this issue, which has never been reported by previous studies.

The lower abundance of M18 between 82 and 90 km as shown in Figure 3 is likely caused by the slower collisional rate of $OH(\nu=8)+O_2$ used in the SABER model, which is about 16 times smaller than laboratory measurements (Dyer et al., 1997). As a result, fewer atomic hydrogen would be needed to model the observed OH emission due to the smaller loss of $OH(\nu=8)$. In contrast, around 96 km, M18 is much higher, which likely arises from the systematic discrepancies between SCIAMACHY and SABER measurements. Zhu et al. (2020) report that the unfiltered OH emissions at 2.0 μ m from SABER are on average 20% higher than those simulated with SCIAMACHY data. Moreover, relative differences can reach 70%–90% at 96 km (Zhu et al., 2020, Figure 4).

The [H] data set derived from Panka et al. (2021) is much higher than those from SCIAMACHY, even when accounting for the uncertainties of our results. Based on our assessment, the 80% discrepancy is primarily caused by the significantly higher excitation of OH(v=9) in the model of Panka et al. (2021). The remaining 20% arises from differences between the [O] and $k_{O_2,9}$ that were taken from Panka et al. (2021) and those in our retrieval. There is a fundamental systematic difference between the approach used by Panka et al. (2021) and the methods employed in other studies that are based on ozone chemical equilibrium. Panka et al. (2021) infer the species (nighttime atomic oxygen and OH(v=1-9) volume mixing ratio) from the ratio of volume emission rates

WU ET AL. 5 of 9

19448007, 2025, 15, Downloaded from https://agupubs.onlinelbrary.wiley.com/doi/10.1029/2025GL116311 by Forschungszentrum Jülich GmbH Research Center, Wiley Online Library on [06:08/2025]. See the Terms and Conditions (https://onlinelbrary.wiley.com/doi/10.1029/2025GL116311 by Forschungszentrum Jülich GmbH Research Center, Wiley Online Library on [06:08/2025]. See the Terms and Conditions (https://onlinelbrary.wiley.com/doi/10.1029/2025GL116311 by Forschungszentrum Jülich GmbH Research Center, Wiley Online Library on [06:08/2025]. See the Terms and Conditions (https://onlinelbrary.wiley.com/doi/10.1029/2025GL116311 by Forschungszentrum Jülich GmbH Research Center, Wiley Online Library on [06:08/2025]. See the Terms and Conditions (https://onlinelbrary.wiley.com/doi/10.1029/2025GL116311 by Forschungszentrum Jülich GmbH Research Center, Wiley Online Library on [06:08/2025]. See the Terms and Conditions (https://onlinelbrary.wiley.com/doi/10.1029/2025GL116311 by Forschungszentrum Jülich GmbH Research Center, Wiley Online Library on [06:08/2025]. See the Terms and Conditions (https://onlinelbrary.wiley.com/doi/10.1029/2025GL116311 by Forschungszentrum Jülich GmbH Research Center, Wiley Online Library on [06:08/2025]. See the Terms and Conditions (https://onlinelbrary.wiley.com/doi/10.1029/2025GL116311 by Forschungszentrum Jülich GmbH Research Center, Wiley Online Library on [06:08/2025]. See the Terms and Conditions (https://onlinelbrary.wiley.com/doi/10.1029/2025GL116311 by Forschungszentrum Jülich GmbH Research Center, Wiley Online Library on [06:08/2025]. See the Terms and Conditions (https://onlinelbrary.wiley.com/doi/10.1029/2025GL116311 by Forschungszentrum Jülich GmbH Research Center, Wiley Online Library on [06:08/2025]. See the Terms and Conditions (https://onlinelbrary.wiley.com/doi/10.1029/2025GL116311 by Forschungszentrum Jülich GmbH Research Center, Wiley Online Library on [06:08/2025]. See the Terms and Conditions (https://onlinelbrary.wiley.com/doi/10.1029/2025GL116311 by Forschungszentrum Jülich GmbH

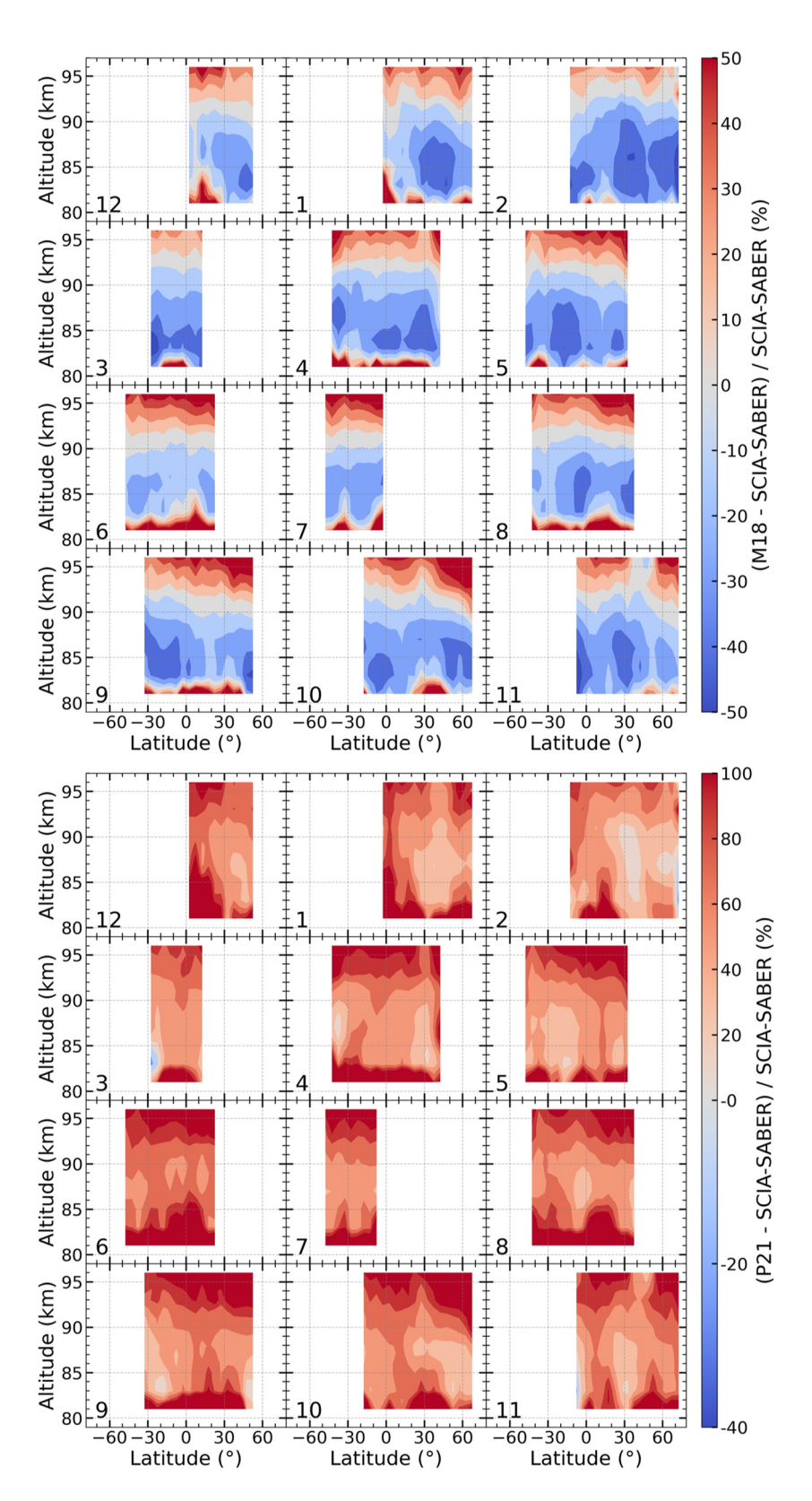


Figure 3. Difference of the zonal mean hydrogen number density data sets for 2005: SCIA-SABER versus M18 (top) and SCIA-SABER versus P21 (bottom). The numbers indicate the months of the year. SCIA-SABER, M18, and P21 are described as in Figure 1.

WU ET AL. 6 of 9

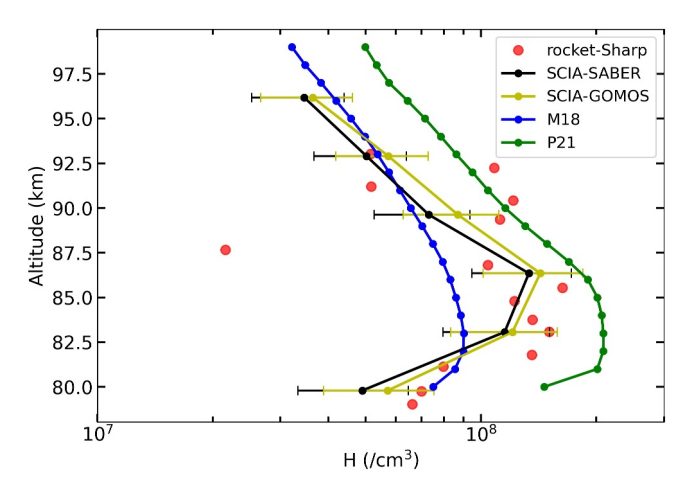


Figure 4. Comparison between the rocket observation of [H] from Sharp and Kita (1987) and the retrieval results from OH airglow observations. The rocket-Sharp represents the [H] data from rocket observation at about 32°N, 106°W, on 7 December 1981, at 18:00 local time. SCIA-SABER, SCIA-GOMOS, M18, and P21 represent the monthly zonal mean [H] for December 2003 at 32°N (±5°), at 22:00 (±1 hr) local time, derived from different models as described in Figure 1.

measured by SABER in channel 2 μm and 1.6 μm , with the dependency on these species entering the retrieval model through relaxation rates. In contrast, the other studies derive the number density of oxygen (and hydrogen) from the chemical excitation of the highest OH vibrational states, where the model is comparatively less influenced by collisional quenching rates. As a result, Panka et al.'s results are far more sensitive to the relaxation model, as it requires accounting for a significantly larger number of transitions compared to the other approach. The two methods also differ in their sensitivity to the radiometric calibration of OH measurements: Panka et al.'s approach depends on the ratio of absolute radiances from the two SABER OH channels, whereas the other methods rely solely on the radiometric calibration of a single OH channel.

Although both the SCIA-GOMOS data set used in this work and the [H] data from Kaufmann et al. (2013) are based on SCIAMACHY OH(9–6) emissions and GOMOS ozone measurements, they differ systematically by about 60%. This discrepancy arises from differences in the background atmospheric data and the model parameters applied. Kaufmann et al. (2013) used a higher quenching rate $k_{O_2,9}$ (3.1 × 10⁻¹¹ cm³/s) and a lower nascent distribution ratio f_9 (0.38), leading to increases of 15% and 32% in the retrieved [H], respectively. The remaining 10%–15% difference between SCIA-GOMOS and the data of Kaufmann et al. (2013) can be explained by the use of

different O_2 background data. Kaufmann et al. (2013) employed O_2 concentrations derived from the MSISE-00 model (Picone et al., 2002) and NCAR ROSE model (Marsh et al., 2001; Smith & Marsh, 2005). The comparison reveals that, between 80 and 96 km, the total density from MSISE-00 is approximately 16%–24% higher than that from SABER, while the O_2 mixing ratio from the NCAR ROSE model is 2%–6% lower than that in MSIS 2.0, which underlies our model. Consequently, the resulting O_2 concentration in Kaufmann et al. (2013) is about 15% higher, leading to an estimated additional 10% increase in the retrieved [H]. This analysis demonstrates that the differences between the data sets of Kaufmann et al. (2013) and this study are largely understood and can be attributed to the use of input data that are now considered outdated. In this context, the SCIA-GOMOS data set presented in this work can be regarded as an updated version of the data published by Kaufmann et al. (2013).

As mentioned earlier, direct (in situ) reference measurements in this altitude range are rare. Sharp and Kita (1987) reported the [H] profile measured by a rocket observation, which is the only direct in situ measurement of [H] to date. Figure 4 compares their rocket observation with retrievals of [H] from OH emission measurements. It shows that the [H] retrieved in this work (black and yellow lines) agrees better with in situ measurements compared to other retrieval results, with most in situ measurements (red dots) deviating by less than 20% from the [H] retrieved in this work. The discrepancies might stem from the fact that the rocket measurements and the OH emission measurements were not made during the same period. Additionally, considering the influence of solar activity, the [H] data sets derived from OH airglow observation that displayed in Figure 4 are 10% higher than that from the rocket observations. It is worth noting that the single rocket measurement may not be sufficient to determine the superiority of one model over another, as the rocket and satellite observations were not conducted under exactly the same solar and seasonal conditions. Moreover, the rocket data may be affected by gravity waves and possible geocoronal emissions, introducing additional uncertainties.

5. Conclusions

Using SCIAMACHY OH(9–6) band data and assuming O_3 chemical equilibrium, we derived a new nighttime atomic hydrogen data set. Since OH($\nu=9$) is predominantly formed through the reaction H + O_3 , our retrieval relies on a minimal set of kinetic and spectroscopic parameters, reducing the uncertainty in the derived [H]. The peak altitude of atomic hydrogen is between 82 and 87 km, with peak concentrations ranging from approximately 1.5×10^8 to 4×10^8 cm⁻³, varying with season and latitude. The results would increase by about 17% if we use hydroxyl Einstein coefficients from HITRAN-2020 instead of those from HITRAN-2012 for retrieval.

In comparison with other [H] data sets, the data from Mlynczak et al. (2018) are about 30% lower than the [H] derived in this work at 82–90 km, primarily due to a lower collisional quenching rate of OH(v = 8) with O_2 used

WU ET AL. 7 of 9

Acknowledgments

No. 1852977.

This work is supported by the Project of

Stable Support for Youth Team in Basic

Research Field, CAS (YSBR-018), the

National Natural Science Foundation of

based upon work supported by the NSF

sponsored by the U.S. National Science

Foundation under Cooperative Agreement

China (42174212), and the Chinese Meridian Project. This material is also

National Center for Atmospheric

Research, which is a major facility

in Mlynczak et al. (2018). Above 90 km, the [H] from Mlynczak et al. (2018) is 10%-50% higher, mainly due to systematic discrepancies between SCIAMACHY and SABER. The [H] data from Panka et al. (2021) are significantly higher than both the data from Mlynczak et al. (2018) and this work, primarily due to the larger density of $OH(\nu=9)$ reported by Panka et al. (2021). Compared to Mlynczak et al. (2018) and Panka et al. (2021), the [H] data retrieved in this study are more consistent with rocket in situ measurements.

Conflict of Interest

The authors declare no conflicts of interest relevant to this study.

Data Availability Statement

The SCIAMACHY Level 1b version 10 data used in this study are available at https://hm-atmos-ds.eo.esa.int/oads/access/collection/Envisat_SCIAMACHY_Level_1b_SCI_____1P/tree. SABER version 2.0 data are available at https://saber.gats-inc.com/browse_data.php. GOMOS Ozone data (Envisat GOMOS Level 2 - Atmospheric constituents profiles - User Friendly Product) used in this study are available at: https://doi.org/10.57780/EN1-dfd0eaa (European Space Agency, 2017). Access requires registration at the ESA Earth Online Portal

References

Adler-Golden, S. (1997). Kinetic parameters for OH nightglow modeling consistent with recent laboratory measurements. *Journal of Geophysical Research*, 102(A9), 19969–19976, https://doi.org/10.1029/97JA01622

Bovensmann, H., Burrows, J. P., Buchwitz, M., Frerick, J., Noël, S., Rozanov, V. V., et al. (1999). SCIAMACHY: Mission objectives and measurement modes. *Journal of the Atmospheric Sciences*, 56(2), 127–150. https://doi.org/10.1175/1520-0469(1999)056(0127:SMOAMM)2.

Burkholder, J. B., Sander, S. P., Abbatt, J. P. D., Barker, J. R., Cappa, C. D., Crounse, J. D., et al. (2020). Chemical kinetics and photochemical data for use in atmospheric studies: Evaluation number 19 (JPL Publication No. 19-5). NASA Jet Propulsion Laboratory. Retrieved from https://www.researchgate.net/publication/343224193_NASA-JPL_Evaluation_19-5

Dyer, M. J., Knutsen, K., & Copeland, R. A. (1997). Energy transfer in the ground state of OH: Measurements of OH (v = 8, 10, 11) removal. *The Journal of Chemical Physics*, 107(19), 7809–7815. https://doi.org/10.1063/1.475094

Emmert, J. T., Drob, D. P., Picone, J. M., Siskind, D. E., Jones, M., Mlynczak, M. G., et al. (2021). NRLMSIS 2.0: A whole-atmosphere empirical model of temperature and neutral species densities. *Earth and Space Science*, 8(3), e2020EA001321. https://doi.org/10.1029/2020EA001321 European Space Agency (2017). Envisat GOMOS level 2 - Atmospheric constituents profiles - User friendly product (GOMOS UPP). (Version

European Space Agency. (2017). Envisat GOMOS level 2 - Atmospheric constituents profiles - User friendly product (GOMOS_UFP), (Version R/IPF 6.01) [Dataset]. European Space Agency. https://doi.org/10.57780/EN1-dfd0eaa

Gordon, I. E., Rothman, L. S., Hargreaves, R. J., Hashemi, R., Karlovets, E. V., Skinner, F. M., et al. (2022). The HITRAN2020 molecular spectroscopic database. *Journal of Quantitative Spectroscopy and Radiative Transfer*, 277, 107949. https://doi.org/10.1016/j.jqsrt.2021. 107949

Gottwald, M., Bovensmann, H., Lichtenberg, G., Noel, S., von Bargen, A., Slijkhuis, S., et al. (2006). In M. Gottwald (Ed.), Sciamachy, monitoring the changing Earth's atmosphere. DLR. Retrieved from https://elib.dlr.de/44026/

Kalogerakis, K. S., Smith, G. P., & Copeland, R. A. (2011). Collisional removal of OH(X²Π, v = 9) by O, O₂, O₃, N₂, and CO₂. *Journal of Geophysical Research*, 116(D20), D20307. https://doi.org/10.1029/2011JD015734

Kaufmann, M., Ern, M., Lehmann, C., & Riese, M. (2013). The response of atomic hydrogen to solar radiation changes. In F.-J. Lübken (Ed.), Climate and weather of the sun-earth system (CAWSES): Highlights from a priority program (pp. 171–188). Springer Netherlands. https://doi. org/10.1007/978-94-007-4348-9 10

Kaufmann, M., Lehmann, C., Hoffmann, L., Funke, B., López-Puertas, M., Savigny, C., & Riese, M. (2008). Chemical heating rates derived from SCIAMACHY vibrationally excited OH limb emission spectra. Advances in Space Research, 41(11), 1914–1920. https://doi.org/10.1016/j.asr. 2007.07.045

Kulikov, M. Y., Belikovich, M. V., Chubarov, A. G., Dementyeva, S. O., & Feigin, A. M. (2023). Boundary of nighttime ozone chemical equilibrium in the mesopause region: Long-term evolution determined using 20-year satellite observations. Atmospheric Chemistry and Physics, 23(22), 14593–14608. https://doi.org/10.5194/acp-23-14593-2023

Kulikov, M. Y., Belikovich, M. V., Chubarov, A. G., Dementyeva, S. O., & Feigin, A. M. (2024). Retrieval of nighttime distributions of mesosphere-lower thermosphere characteristics from satellite data. *Izvestiya*, Atmospheric and Oceanic Physics, 60(1), 74–86. https://doi.org/ 10.1134/S0001433824700051

Kulikov, M. Y., Belikovich, M. V., Grygalashvyly, M., Sonnemann, G. R., & Feigin, A. M. (2022). Retrieving daytime distributions of O, H, OH, HO_2 , and chemical heating rate in the mesopause region from satellite observations of ozone and OH^* volume emission: The evaluation of the importance of the reaction $H + O_3 \rightarrow O_2 + OH$ in the ozone balance. Advances in Space Research, 69(9), 3362–3373. https://doi.org/10.1016/j.asr.2022.02.011

 $Lacoursi\`ere, J., Dyer, M. J., \& Copeland, R. A. (2003). Temperature dependence of the collisional energy transfer of OH(v=10) between 220 and 310 K. \textit{The Journal of Chemical Physics, } 118(4), 1661–1666. https://doi.org/10.1063/1.1530581$

Marsh, D., Smith, A., Brasseur, G., Kaufmann, M., & Grossmann, K. (2001). The existence of a tertiary ozone maximum in the high-latitude middle mesosphere. Geophysical Research Letters, 28(24), 4531–4534. https://doi.org/10.1029/2001GL013791

Mlynczak, M. G., Hunt, L. A., Marshall, B. T., Mertens, C. J., Marsh, D. R., Smith, A. K., et al. (2014). Atomic hydrogen in the mesopause region derived from SABER: Algorithm theoretical basis, measurement uncertainty, and results. *Journal of Geophysical Research: Atmospheres*, 119(6), 3516–3526. https://doi.org/10.1002/2013JD021263

Mlynczak, M. G., Hunt, L. A., Russell III, J. M., & Marshall, B. T. (2018). Updated SABER night atomic oxygen and implications for SABER ozone and atomic hydrogen. Geophysical Research Letters, 45(11), 5735–5741. https://doi.org/10.1029/2018GL077377

WU ET AL. 8 of 9

- Mlynczak, M. G., & Solomon, S. (1991). Middle atmosphere heating by exothermic chemical reactions involving odd-hydrogen species. Geophysical Research Letters, 18(1), 37–40. https://doi.org/10.1029/90GL02672
- Mlynczak, M. G., & Solomon, S. (1993). A detailed evaluation of the heating efficiency in the middle atmosphere. *Journal of Geophysical Research*, 98(D6), 10517–10541. https://doi.org/10.1029/93JD00315
- Panka, P. A., Kutepov, A. A., Kalogerakis, K. S., Janches, D., Russell, J. M., Rezac, L., et al. (2017). Resolving the mesospheric nighttime 4.3 μm emission puzzle: Comparison of the CO₂ (ν₃) and OH (ν) emission models. *Atmospheric Chemistry and Physics*, 17(16), 9751–9760. https://doi.org/10.5194/acp-17-9751-2017
- Panka, P. A., Kutepov, A. A., Zhu, Y., Kaufmann, M., Kalogerakis, K. S., Rezac, L., et al. (2021). Simultaneous retrievals of nighttime O (³P) and total OH densities from satellite observations of Meinel band emissions. *Geophysical Research Letters*, 48(1), e2020GL091053. https://doi.org/10.1029/2020GL091053
- Picone, J. M., Hedin, A. E., Drob, D. P., & Aikin, A. C. (2002). NRLMSISE-00 empirical model of the atmosphere: Statistical comparisons and scientific issues. *Journal of Geophysical Research*, 107(A12). SIA 15-1–SIA 15-16. https://doi.org/10.1029/2002JA009430
- Rothman, L. S., Gordon, I. E., Babikov, Y., Barbe, A., Benner, C. D., Bernath, P. F., et al. (2013). The HITRAN2012 molecular spectroscopic database. *Journal of Quantitative Spectroscopy and Radiative Transfer*, 130, 4–50. https://doi.org/10.1016/j.jqsrt.2013.07.002
- Sharma, R. D., Wintersteiner, P. P., & Kalogerakis, K. S. (2015). A new mechanism for OH vibrational relaxation leading to enhanced CO₂ emissions in the nocturnal mesosphere. Geophysical Research Letters, 42(11), 4639–4647. https://doi.org/10.1002/2015GL063724
- Sharp, W. E., & Kita, D. (1987). In situ measurement of atomic hydrogen in the upper mesosphere. *Journal of Geophysical Research*, 92(D4), 4319–4324. https://doi.org/10.1029/JD092iD04p04319
- Smith, A. K., & Marsh, D. R. (2005). Processes that account for the ozone maximum at the mesopause. *Journal of Geophysical Research*, 110(D23), 2005JD006298. https://doi.org/10.1029/2005JD006298
- Xu, J., Gao, H., Smith, A. K., & Zhu, Y. (2012). Using TIMED/SABER nightglow observations to investigate hydroxyl emission mechanisms in the mesopause region. *Journal of Geophysical Research*, 117(D2), D02301. https://doi.org/10.1029/2011JD016342
- Zhu, Y., & Kaufmann, M. (2018). Atomic oxygen abundance retrieved from SCIAMACHY hydroxyl nightglow measurements. Geophysical Research Letters, 45(17), 9314–9322. https://doi.org/10.1029/2018GL079259
- Zhu, Y., Kaufmann, M., Chen, Q., Xu, J., Gong, Q., Liu, J., et al. (2020). A comparison of OH nightglow volume emission rates as measured by SCIAMACHY and SABER. *Atmospheric Measurement Techniques*, 13(6), 3033–3042. https://doi.org/10.5194/amt-13-3033-2020

WU ET AL. 9 of 9